

# Strong Spin-Motion Coupling in the Ultrafast Quantum Many-body Dynamics of Rydberg Atoms in a Mott-insulator Lattice

V. Bharti,<sup>1,\*</sup> S. Sugawa,<sup>1,2,3</sup> M. Kunimi,<sup>4</sup> V. S. Chauhan,<sup>1</sup> T. P. Mahesh,<sup>1,2</sup> M. Mizoguchi,<sup>1</sup> T. Matsubara,<sup>1</sup> T. Tomita,<sup>1,2</sup> S. de Léséleuc,<sup>1,2,†</sup> and K. Ohmori<sup>1,2,‡</sup>

<sup>1</sup>*Institute for Molecular Science, National Institutes of Natural Sciences, Okazaki 444-8585, Japan*

<sup>2</sup>*SOKENDAI (The Graduate University for Advanced Studies), Okazaki 444-8585, Japan*

<sup>3</sup>*Department of Basic Science, The University of Tokyo, Meguro-ku, Tokyo, 153-8902, Japan*

<sup>4</sup>*Department of Physics, Tokyo University of Science, Shinjuku-ku, Tokyo, 162-8601, Japan*

(Dated: November 28, 2023)

Rydberg atoms in optical lattices and tweezers is now a well established platform for simulating quantum spin systems. However, the role of the atoms' spatial wavefunction has not been examined in detail experimentally. Here, we show a strong spin-motion coupling emerging from the large variation of the interaction potential over the wavefunction spread. We observe its clear signature on the ultrafast, out-of-equilibrium, many-body dynamics of atoms excited to a Rydberg  $S$  state from an unity-filling atomic Mott-insulator. We also propose a novel approach to tune arbitrarily the strength of the spin-motion coupling relative to the motional energy scale set by trapping potentials. Our work provides a new direction for exploring the dynamics of strongly-correlated quantum systems by adding the motional degree of freedom to the Rydberg simulation toolbox.

Quantum simulation platforms, such as ion crystals [1], polar molecules [2], ultracold neutral atoms [3], and Rydberg atoms [4], offer remarkable opportunities to study various many-body problems, of which one important category are localized spin models, see e.g. [5–9]. To mimic pure spin systems, two energy levels in the internal degrees of freedom (d.o.f.) are identified as an effective spin-1/2, and approximations are then applied onto the full Hamiltonian describing a given experimental platform, notably to decouple the external motional d.o.f. (position and momentum) from the spin dynamics. Recently, new proposals are emerging to purposely use *spin-motion coupling* (i.e., a state-dependent force) and open new regimes of quantum simulation with Rydberg atoms [10–14]. In this work, based on the ultrafast Rydberg quantum platform [15, 16], we report on the experimental realization of an extreme regime of spin-motion coupling  $\kappa$  which is (i) comparable to the spin-spin interaction strength  $V$ , and (ii) overly dominates the natural motional energy scale  $\omega$  set by a trapping potential. We also propose a novel experimental approach, *ultrafast stroboscopic Rydberg excitation*, to tune the ratio  $\kappa/\omega$  over many orders of magnitude.

Rydberg atoms display interactions ranging up to the GHz-scale at micrometer inter-atomic distances  $r$  [4, 17]. The potential  $V(r)$  typically follows a  $1/r^3$ -dependence for resonant dipole-dipole interaction, or a  $1/r^6$ -potential in the non-resonant van der Waals (vdW) regime. Over the last decade, spin models have been implemented with Rydberg atoms in a gas phase [18–20], in an optical lattice [16, 21, 22], or in an array of optical tweezers, e.g. [8, 9, 23, 24]. In these works, spin-motion coupling (arising when the atom explores the spatially-varying potential) is either considered negligible, or as a small source of decoherence with the external degrees of freedom treated as a thermal bath. For example, if atoms

move randomly during the dynamics, because of a finite thermal energy, the interaction varies and blurs the spin dynamics. By preparing atoms in a pure motional quantum state, the coupling to motion is coherent and creates spin-motion entanglement [15].

In this coherent regime, the spin-motion coupling originates from the variation of the potential  $V(r)$  over the rms (root mean squared) spread  $x_{\text{rms}}$  of the atom position wavefunction, around a distance  $d$  [13]. The first-order, linear, spin-motion coupling term is parameterized by  $\kappa$ :

$$\kappa = -x_{\text{rms}} \left. \frac{\partial V}{\partial x} \right|_{x=d} = 6 \frac{x_{\text{rms}}}{d} V(d), \quad (1)$$

where we assumed a repulsive vdW potential. First, we compare the ratio of spin-motion to spin-spin coupling  $\kappa/V$ , which depends on the choice of optical traps: lattice or tweezers. In both approaches, the quantum fluctuation of position  $x_{\text{rms}} = \sqrt{\hbar/2m\omega}$  ( $m$  the mass of the atom) is slightly tunable through the trapping angular frequency  $\omega \sim 2\pi \times 10 - 100$  kHz giving a spread of a few tens of nanometers. The distance  $d$  between atoms is typically  $0.5 \mu\text{m}$  with lattice and can range from  $2$  to  $10 \mu\text{m}$  for tweezers. Consequently, the spin-motion coupling is usually only a small perturbation for tweezers  $\kappa/V \ll 0.1$  [15], while it is comparable to the spin-spin coupling in the lattice platform  $\kappa/V \sim 0.5$ . We will see clear signatures of this large perturbation on the spin dynamics in the first part of this work.

Secondly, we discuss the relevance of motion through the ratio  $\kappa/\omega$ , which can vary over many orders of magnitude depending on the platform. For molecules, interacting through a dipole-dipole potential  $V$  on the kHz-scale or less [6, 25, 26], the spin-motion coupling is negligible  $\kappa/\omega < 0.01$ , except if working with delocalized, overlapping, wavefunctions [27]. For Rydberg atoms excited with cw-lasers, forcing the Rydberg blockade limits the

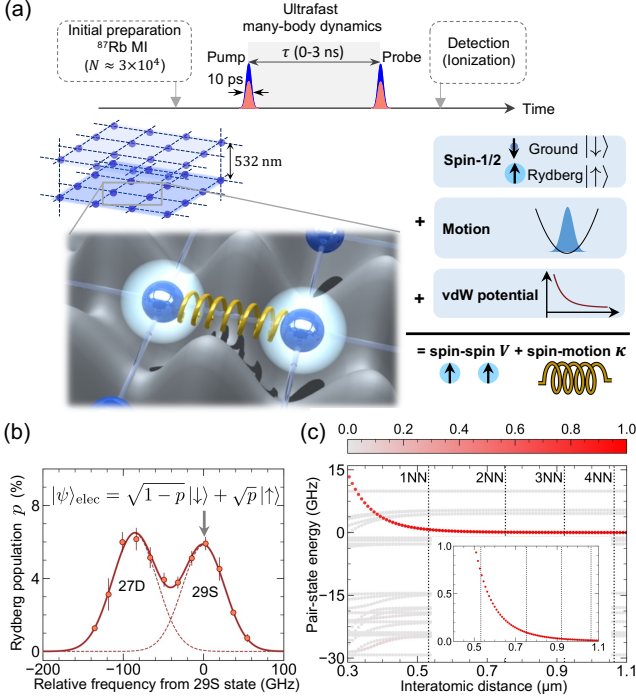


FIG. 1. (a) Schematic of the experiment. The atoms prepared in a unity-filling 3D atomic Mott-insulator are coherently excited to the  $29S$  Rydberg state using a pump pulse. After the pump excitation, the system undergoes many-body dynamics driven by spin-spin and spin-motion couplings until the probe pulse is applied. (b) Rydberg state population after excitation with a pulse of 10 picoseconds. The solid curve shows a fit by a double Gaussian function, while the dashed curves represent the individual contribution from the state  $27D$  and  $29S$ . (c) The  $29S-29S$  pair state energy as a function of inter-atomic distance, showing a repulsive vdW potential. The inset zooms in the  $0-1$  GHz energy range.

interaction strength  $V$  to the MHz-scale which nevertheless allows to enter the perturbative regime  $\kappa/\omega \sim 0.1-0.5$  and already opens up exciting prospects [11–14]. By using picosecond pulsed lasers, our ultrafast approach allows to always overcome Rydberg blockade [28] and prepare Rydberg atoms with interaction strength at the GHz-scale [15, 16, 18]. Here, the spin-motion coupling becomes overly dominant with  $\kappa/\omega \sim 10-1000$ , such that motional dynamics can be completely neglected on the timescale of spin-spin and spin-motion entanglement. In the final part of this work, we will propose the ultrafast stroboscopic method to effectively tune  $\kappa/\omega$ .

*Experimental platform* The schematic of our experimental system is shown in Fig. 1(a). We prepare a three-dimensional (3D) unity-filling Mott-insulator state with  $\sim 3 \times 10^4$  atoms in the  $|\downarrow\rangle = |5S\rangle$  ground state of  $^{87}\text{Rb}$ . The 3D optical lattice, with period  $a_{\text{lat}} = 532$  nm, has a depth of  $20 E_R$  for each axis giving rise to an isotropic trapping frequency  $\omega = 2\pi \times 18$  kHz in the harmonic oscillator approximation (for details, see Ref. [16]). The

spatial wavefunction  $|\psi\rangle_{\text{spatial}}$  of each atom have a quantum uncertainty of position  $x_{\text{rms}} = 57$  nm, and a momentum uncertainty  $p_{\text{rms}} = \hbar/2x_{\text{rms}} = m \times (6.4$  mm/s).

Following preparation of the ground-state atoms, they are then coherently excited to the  $|\uparrow\rangle = |29S\rangle$  Rydberg state using a two-photon excitation with broadband laser pulses as described in Ref. [29] and shown in Fig. 1(b). This prepares each atom in a coherent electronic superposition  $|\psi\rangle_{\text{elec}} = \sqrt{1-p}|\downarrow\rangle + \sqrt{p}|\uparrow\rangle$ , with  $p$  the probability to be in the Rydberg state, and where we mapped the ground and Rydberg states to a spin-1/2. Two atoms in the  $29S$  state experience strong dipole-dipole interaction in the vdW regime. Figure 1(c) shows the interaction potential calculated using the pairinteraction software [30, 31]. It is very well approximated by an isotropic, repulsive, vdW form  $V(r) = C_6/r^6$ , where the calculated coefficient  $C_6^{\text{th}}$  is  $2\pi \times 16$  MHz  $\mu\text{m}^6$ . At the shortest inter-atomic distance, the interaction is expected to be 0.7 GHz. The mixing with the dominant interaction channel (the pair-state  $28P-29P$ ) remains negligible thanks to its large energy separation of 20 GHz. Choosing a Rydberg  $S$ -state, rather than  $D$ -state as in previous works [15, 16], was motivated by obtaining this clean isotropic potential, despite the increased experimental challenge caused by the smaller excitation strength of  $S$ -state and in spectrally resolving the  $S$  and  $D$  states when using picosecond laser pulses [29].

*The model Hamiltonian* Here, we discuss the model Hamiltonian, including the motional degrees of freedom. Following excitation, each atom  $j$  is initially in a product state of spatial and internal d.o.f.  $|\psi_j\rangle = |\psi\rangle_{\text{spatial}} \otimes |\psi\rangle_{\text{elec}}$ . We then consider the evolution of this system in the nanosecond timescale relevant for spin-spin and spin-motion entanglement. For such short duration, the motion of atoms can be completely ignored: the position probability distribution do not have time to evolve either from the absence of confining potential for the Rydberg state or from the vdW repulsion. The ultrafast dynamics is then driven only by:

$$\begin{aligned} \frac{\hat{H}}{\hbar} &= \sum_{j < k} V(\hat{\mathbf{r}}_{jk}) \otimes \hat{n}_j \hat{n}_k \\ &\approx \sum_{j < k} \left( V_{jk} + \kappa_{jk} \frac{\hat{\mathbf{r}}_{jk} - \bar{\mathbf{r}}_{jk}}{x_{\text{rms}}} \cdot \mathbf{e}_{jk} + \dots \right) \otimes \hat{n}_j \hat{n}_k. \end{aligned} \quad (2)$$

Here,  $\hat{\mathbf{r}}_{jk} = \hat{\mathbf{r}}_j - \hat{\mathbf{r}}_k$  is the quantum operator of the relative position of atoms  $j$  and  $k$ ,  $\bar{\mathbf{r}}_{jk}$  its expectation value,  $\mathbf{e}_{jk}$  a unit vector along site  $j$  and  $k$ ,  $V_{jk}$  and  $\kappa_{jk}$  the couplings evaluated at distance  $\bar{r}_{jk}$ , and  $\hat{n}_j = |\uparrow\rangle_j \langle \uparrow|$  is the projection operator on the Rydberg state for the  $j$ -th atom. Applying this Hamiltonian to the initial product state creates entanglement within the spin sector, but also, and this is the key point of the first part of this work, between the spin and motional sectors of the Hilbert space. In the second line of Eq. (2), we perform

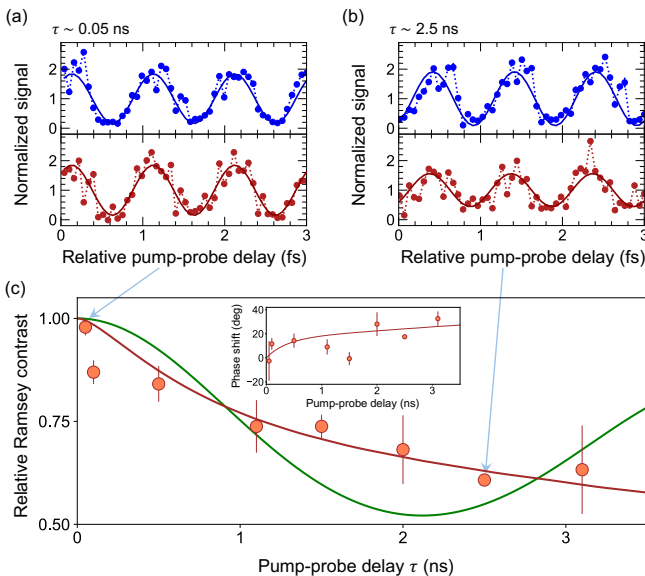


FIG. 2. Time-domain Ramsey interferograms for atoms prepared in a Mott-insulator, strongly-interacting, state (red) and a low-density, non-interacting, reference atomic sample (blue) for (a)  $\tau \sim 0.05$  ns and (b)  $\tau \sim 2.5$  ns. (c) Measured relative Ramsey contrasts and phase shifts are shown by red circles (error bars are standard error of the mean). The observations are compared with a fitted numerical solution (with  $C_6$  as the only free parameter) that takes into account spin-motion coupling (red curve) or ignore it (green curve).

an expansion of the potential up to first-order, useful for a later qualitative discussion and to outline the appearance of spin-motion coupling parametrized by  $\kappa$ .

*Results* We now present experimental results obtained by time-domain Ramsey interferometry [15, 16, 18], to probe the many-body entangled state generated by the above Hamiltonian. In short, a first pump pulse initiates the many-body dynamics which is read-out by a second probe pulse after a variable delay  $\tau = 0 - 3$  ns. This second pulse gives rise to a Ramsey interference whose contrast is a probe to the single-atom coherence in the spin sector, i.e., between the ground and Rydberg state. Spin-spin and spin-motion coupling generates entanglement entropy [16], which reduces the single-atom coherence and thus the Ramsey contrast. Typical interferograms are shown in Fig. 2(a,b). In absence of interaction (blue curve, obtained for a low-density atomic sample), the highly contrasted interference indicates a constant pure state. For atoms prepared as a Mott-insulator (red curve), the decreasing contrast signals a reduced purity in the spin sector, which is shown in Fig. 2(c) as a function of the delay  $\tau$ . Additionally, we also extract a phase shift of the Ramsey oscillations with the reference non-interacting sample.

*Numerical solution* To calculate the Ramsey contrast and phase shift from the action of the Hamiltonian of Eq. (2), we extend previous results [18, 32] to include

the spatial wavefunction of each atom, which requires to calculate terms such as the two-body spatial overlap:

$$O_{jk}(t) = \langle \psi_j; \psi_k | \exp(-iV(\hat{\mathbf{r}})t) | \psi_j; \psi_k \rangle \\ = C \int d\mathbf{r} \exp\left(-\frac{|\mathbf{r} - \bar{\mathbf{r}}_{jk}|^2}{x_{\text{rms}}^2} - i\frac{C_6}{|\mathbf{r}|^6}t\right), \quad (3)$$

where  $C$  is a normalization constant. The second line is obtained after reformulating the two-body wavefunctions  $|\psi_j; \psi_k\rangle$  into two independent one-body system: a trivial one for the center-of-mass, unaffected by the interaction, and the interesting one for the relative coordinate  $\mathbf{r}_{jk}$  with reduced mass  $m/2$ . For a two-atom system, the Ramsey contrast and phase are directly related to the amplitude and phase of the complex-valued overlap  $O$ . For the many-body dynamics considered here, the analytical expression relating them is given in Ref. [29], which also include details on neglecting three-body (and higher) overlap terms.

The calculation results are then fitted to the Ramsey contrast data with a single free parameter: the coefficient  $C_6$ . The fitted curve, see Fig. 2(c), agrees well with the experimental data for a coefficient  $C_6^{\text{exp}} = 2\pi \times 5.5 \text{ MHz } \mu\text{m}^6$ . With this value, the positive trend (related to the sign of  $C_6$ ) and magnitude of the phase shift are also well captured. The fitted  $C_6^{\text{exp}}$  coefficient is 3 times smaller than obtained from ab-initio calculation of the vdW potential, which calls for further investigation of the accuracy of the vdW potential calculation in the short, sub-micron distance regime. This could be done using a tweezers platform where a simpler system of only two atoms can be prepared [15], potentially down to the short sub-micrometer distance explored here by throwing atoms with moving tweezers [33].

To emphasize the importance of the spin-motion coupling in this experiment, we also show calculation for a pure spin-spin model where we ignore the spatial extent of the wavefunctions, as done in previous works [16, 18]. As shown in the green curve of Fig. 2(c), the Ramsey contrast would have displayed an oscillation which is clearly absent in the experimental data. We can thus conclude that capturing spin-motion entanglement is essential to account for the observed many-body dynamics.

*Discussion* We now present a hierarchy of approximations to identify the relevant terms in Eqs. (2,3) that create spin-motion entanglement. We consider two atoms at nearest-neighbour (NN) distance  $a_{\text{lat}}$ , where the variation of potential over the wavefunction describing their relative distance  $\psi_{12}(\mathbf{r})$  is largest. We then restrict the problem to 1D, along the inter-atomic axis, by neglecting the wavefunction spread in the other two directions as it gives a small  $\frac{1}{2}(x_{\text{rms}}/a_{\text{lat}})^2 \simeq 0.5\%$  increase in nearest-neighbor distance, 20 times smaller than the effect along the inter-atomic axis. This allows a convenient phase-space representation of the 1D wavefunction  $\psi_{12}(x)$ , as shown in Fig. 3(a).

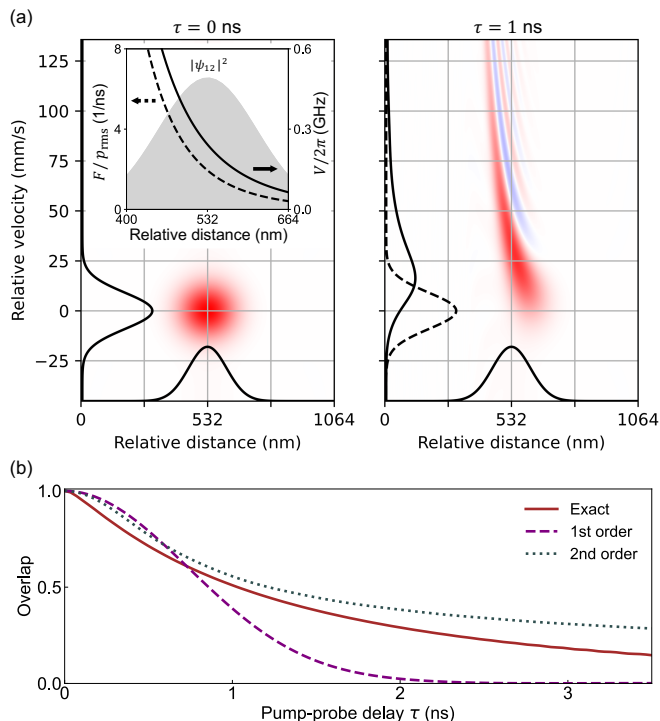


FIG. 3. (a) Phase-space (Wigner) representation of the relative wavefunction  $\psi_{12}$  at time  $\tau = 0$  and 1 ns. The red (blue) color represents positive (negative) value of the Wigner distribution. The marginal position and velocity distribution are shown as black lines. The momentum displacement and squeezing are clearly visible. Inset: zoom on the probability distribution  $|\psi_{12}|^2$ , showing the spatial variation of the vdW potential  $V$  (solid), and the resulting force  $F$  (dashed). (b) Overlap  $|O(t)|$  as a function of the delay  $\tau$ . Solid curve: exact calculation of Eq. (3). The dashed (dotted) lines are obtained by expanding the vdW potential to first-order (second-order).

The  $1/r^6$ -potential then applies a strong force on the wavefunction which can be decomposed with a series expansion of the potential around the mean interatomic distance  $a_{\text{lat}}$ . The zeroth-order term  $V = C_6^{\text{exp}}/a_{\text{lat}}^6$  gives rise to spin-spin entanglement reaching its maximal value at time  $\tau = \pi/V = 2.1$  ns, and corresponding to a minimum in the Ramsey contrast of the green curve of Fig. 2(c). For longer time, the two effective spins would de-entangle and the Ramsey visibility re-increase [15, 34]. The first-order linear term, explicitly written in Eq. (2), gives a uniform force on the wavefunction  $F = 6\hbar C_6/a_{\text{lat}}^7 = \hbar\kappa/x_{\text{rms}} \simeq \frac{m}{2}(2.5 \times 10^7 \text{ m s}^{-2})$ . The momentum kick  $\Delta p$  from this acceleration becomes comparable to the relative momentum rms spread after  $\tau = p_{\text{rms}}/\sqrt{2F} = 0.3$  ns. As the state-dependent force is applied only on part of the spin sector ( $|\uparrow\uparrow\rangle$ ), it creates spin-motion entanglement that is captured by the reduced overlap  $|O|$  between the displaced and initial momentum wavefunction seen in Fig. 3(b). It explains why the Ramsey contrast drops initially faster than expected from a pure spin model, see Fig. 2(c), as well as why it

does not re-increase beyond  $\tau = 2.1$  ns as the pure spin model predicts.

For a good qualitative description of the dynamics, it is necessary to go beyond the first-order term to capture the wide variation of the mechanical force over the wavefunction. As seen in Fig. 3(b), a second-order expansion brings the calculated overlap much closer to the exact result from Eq. (3). Qualitatively, these second-order terms  $\hat{x}_j^2 = (\hat{x}_j - \hat{x}_k)^2$  have two interesting effects on the wavefunction. First, they squeeze each atom wavefunction through the terms  $\hat{x}_j^2$  and  $\hat{x}_k^2$ : the atoms feel a stronger force at shorter distance from the other one, which will compress the wavefunction. And secondly, they entangle the two atoms wavefunctions through the cross term  $\hat{x}_j\hat{x}_k$ . The relative wavefunction  $\psi_{12}$  cannot anymore be decomposed into a product state of two single-atom wavefunctions. Such entanglement between the motion of two atoms is not captured at lower order. The third-order terms are required to explain the negative value taken by the Wigner distribution.

*Outlook* The strong spin-motion coupling observed here precludes the realization of a pure spin model in our experimental regime. However, instead of performing quantum simulation in the spin sector, we could rather work fully in the motion sector of the Hilbert space. This would be realized by completely transferring ground-state atoms to Rydberg orbits, a step that can be done with high-fidelity in the microsecond timescale [35] (but only for weakly interacting atoms), and for which progress have been reported by our group for picosecond-scale excitation [15]. We could then prepare a unit-filling Mott-insulator state of *Rydberg* atoms which would be submitted to strong internal vdW force [36]. Interestingly, the forces from two opposite directions of a given atom cancel in first-order and the second-order squeezing and entangling terms would dominate the dynamics. This would lead to non-trivial distortion of the spatial wavefunctions observable by time-of-flight imaging, a technique also available on the tweezers platform [37, 38].

In this work, we neglected the effect of kinetic energy due to the large separation of timescales between the Rydberg interaction (nanoseconds) and the motion of atoms (microseconds). We now propose to bring these two scales together to investigate a larger class of Hamiltonians with *ultrafast stroboscopic Rydberg excitation*. As schematically drawn in Fig. 4, ground-state atoms are transferred in a picosecond-timescale to Rydberg states to experience for a brief time  $T_R$  the strong force demonstrated in this work. They are then brought back to the ground-state to now experience the kinetic energy and the trapping potential on a microsecond-timescale  $T_0$ . This step is repeated with a high enough frequency to apply Average Hamiltonian Theory (AHT) [39–42], and a controlled duty cycle to vary the effective, reduced, coupling strength  $\kappa_{\text{eff}} = T_R/T_0 \times \kappa$  relatively to the trapping frequency  $\omega$ . Optionally, a spin-1/2 can be encoded in

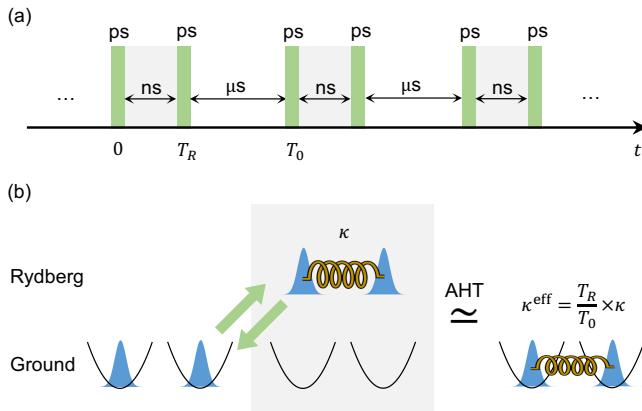


FIG. 4. Hamiltonian engineering by *ultrafast stroboscopic Rydberg excitation*. (a) Pulse sequence, see text. (b) The stroboscopic sequence gives rise to an average Hamiltonian with tunable interaction strength competing with the trapping potential.

the ground-state manifold, and a spin-dependent force obtained by spin-selective ultrafast excitation.

This ultrafast Floquet engineering approach can be seen as complementary to Rydberg dressing [19, 21, 24, 43, 44], where a trapped ground-state atom is instead continuously and weakly dressed by a small fraction of Rydberg character. Compared to other proposals for spin-motion coupling using long-lived circular Rydberg states [14], or Rydberg facilitation (anti-blockade) [11–13], here we note that the stroboscopic approach have the practical advantage to not require magic-trapping of the Rydberg state. Finally, we emphasize that ultrafast Rydberg excitation with pulsed lasers (delivering up to 100 GHz of ground-Rydberg Rabi frequency) unlocks the full GHz-strength of interaction between Rydberg atoms, otherwise curbed by the limited MHz-scale Rabi frequency achievable with cw-lasers.

In conclusion, we have considered the force experienced by Rydberg atoms, mapped it into a spin-motion coupling term, and observed a clear signature: a strong perturbation to the spin dynamics. We proposed a quantum control technique, ultrafast Floquet engineering, to tune the relative strength of this force compared to the trapping potential of optical lattice or tweezers, opening novel regimes of quantum simulation with Rydberg atoms. Among the new avenues, we envision the creation of exotic motional states such as a Rydberg crystal: an atomic array with each atom stabilized in free-space (i.e., in the absence of a confining lattice potential) by long-range isotropic vdW repulsion between Rydberg atoms, a state reminiscent of electronic Wigner crystals [45].

The authors acknowledge Y. Okano and H. Chiba for the technical support. We thank Y. Zhang for the helpful discussions regarding the extension of delay line. This work was supported by MEXT Quantum Leap Flagship Program (MEXT Q-LEAP) JPMXS0118069021, JSPS

Grant-in-Aid for Specially Promoted Research Grant No. 16H06289 and JST Moonshot R&D Program Grant Number JPMJMS2269. S.S. acknowledges support from JSPS KAKENHI Grant No. JP21H01021. M.K. acknowledges supports from JSPS KAKENHI Grants No. JP20K14389 and No. JP22H05268.

\* vineet@ims.ac.jp

† sylvain@ims.ac.jp

‡ ohmori@ims.ac.jp

- [1] C. Monroe, W. C. Campbell, L.-M. Duan, Z.-X. Gong, A. V. Gorshkov, P. W. Hess, R. Islam, K. Kim, N. M. Linke, G. Pagano, P. Richerme, C. Senko, and N. Y. Yao, Programmable quantum simulations of spin systems with trapped ions, *Rev. Mod. Phys.* **93**, 025001 (2021).
- [2] T. Langen, G. Valtolina, D. Wang, and J. Ye, Quantum state manipulation and science of ultracold molecules (2023), arXiv:2305.13445 [cond-mat.quant-gas].
- [3] C. Gross and I. Bloch, Quantum simulations with ultracold atoms in optical lattices, *Science* **357**, 995 (2017).
- [4] A. Browaeys and T. Lahaye, Many-body physics with individually controlled Rydberg atoms, *Nature Physics* **16**, 132 (2020).
- [5] M. K. Joshi, F. Kranzl, A. Schuckert, I. Lovas, C. Maier, R. Blatt, M. Knap, and C. F. Roos, Observing emergent hydrodynamics in a long-range quantum magnet, *Science* **376**, 720 (2022).
- [6] B. Yan, S. A. Moses, B. Gadway, J. P. Covey, K. R. Hazard, A. M. Rey, D. S. Jin, and J. Ye, Observation of dipolar spin-exchange interactions with lattice-confined polar molecules, *Nature* **501**, 521 (2013).
- [7] P. N. Jepsen, J. Amato-Grill, I. Dimitrova, W. W. Ho, E. Demler, and W. Ketterle, Spin transport in a tunable Heisenberg model realized with ultracold atoms, *Nature* **588**, 403 (2020).
- [8] G. Semeghini, H. Levine, A. Keesling, S. Ebadi, T. T. Wang, D. Bluvstein, R. Verresen, H. Pichler, M. Kalinowski, R. Samajdar, A. Omran, S. Sachdev, A. Vishwanath, M. Greiner, V. Vuletić, and M. D. Lukin, Probing topological spin liquids on a programmable quantum simulator, *Science* **374**, 1242 (2021).
- [9] C. Chen, G. Bornet, M. Bintz, G. Emperauger, L. Leclerc, V. S. Liu, P. Scholl, D. Barredo, J. Hauschild, S. Chatterjee, M. Schuler, A. M. Läuchli, M. P. Zaletel, T. Lahaye, N. Y. Yao, and A. Browaeys, Continuous symmetry breaking in a two-dimensional Rydberg array, *Nature* **616**, 691 (2023).
- [10] R. Belyansky, J. T. Young, P. Bienias, Z. Eldredge, A. M. Kaufman, P. Zoller, and A. V. Gorshkov, Nondestructive cooling of an atomic quantum register via state-insensitive Rydberg interactions, *Phys. Rev. Lett.* **123**, 213603 (2019).
- [11] F. M. Gambetta, W. Li, F. Schmidt-Kaler, and I. Lesanovsky, Engineering nonbinary Rydberg interactions via phonons in an optical lattice, *Phys. Rev. Lett.* **124**, 043402 (2020).
- [12] P. P. Mazza, R. Schmidt, and I. Lesanovsky, Vibrational dressing in kinetically constrained Rydberg spin systems, *Phys. Rev. Lett.* **125**, 033602 (2020).
- [13] M. Magoni, R. Joshi, and I. Lesanovsky, Molecular dy-

- namics in Rydberg tweezer arrays: Spin-phonon entanglement and Jahn-Teller effect, *Phys. Rev. Lett.* **131**, 093002 (2023).
- [14] P. Méhaignerie, C. Sayrin, J.-M. Raimond, M. Brune, and G. Roux, Spin-motion coupling in a circular-Rydberg-state quantum simulator: Case of two atoms, *Phys. Rev. A* **107**, 063106 (2023).
- [15] Y. Chew, T. Tomita, T. P. Mahesh, S. Sugawa, S. de Léséleuc, and K. Ohmori, Ultrafast energy exchange between two single Rydberg atoms on the nanosecond timescale, *Nature Photonics* **16**, 724 (2022).
- [16] V. Bharti, S. Sugawa, M. Mizoguchi, M. Kunimi, Y. Zhang, S. de Léséleuc, T. Tomita, T. Franz, M. Weidemüller, and K. Ohmori, Picosecond-scale ultrafast many-body dynamics in an ultracold Rydberg-excited atomic Mott insulator, *Phys. Rev. Lett.* **131**, 123201 (2023).
- [17] M. Saffman, T. G. Walker, and K. Mølmer, Quantum information with Rydberg atoms, *Rev. Mod. Phys.* **82**, 2313 (2010).
- [18] N. Takei, C. Sommer, C. Genes, G. Pupillo, H. Goto, K. Koyasu, H. Chiba, M. Weidemüller, and K. Ohmori, Direct observation of ultrafast many-body electron dynamics in an ultracold Rydberg gas, *Nature communications* **7**, 13449 (2016).
- [19] V. Borish, O. Marković, J. A. Hines, S. V. Rajagopal, and M. Schleier-Smith, Transverse-field Ising dynamics in a Rydberg-dressed atomic gas, *Phys. Rev. Lett.* **124**, 063601 (2020).
- [20] A. Signoles, T. Franz, R. Ferracini Alves, M. Gärttner, S. Whitlock, G. Zürn, and M. Weidemüller, Glassy dynamics in a disordered Heisenberg quantum spin system, *Phys. Rev. X* **11**, 011011 (2021).
- [21] J. Zeiher, R. Van Bijnen, P. Schauß, S. Hild, J.-y. Choi, T. Pohl, I. Bloch, and C. Gross, Many-body interferometry of a Rydberg-dressed spin lattice, *Nature Physics* **12**, 1095 (2016).
- [22] E. Guardado-Sanchez, P. T. Brown, D. Mitra, T. Devakul, D. A. Huse, P. Schauß, and W. S. Bakr, Probing the quench dynamics of antiferromagnetic correlations in a 2d quantum Ising spin system, *Phys. Rev. X* **8**, 021069 (2018).
- [23] K. Kim, F. Yang, K. Mølmer, and J. Ahn, Realization of an extremely anisotropic Heisenberg magnet in Rydberg atom arrays (2023), arXiv:2307.04342 [quant-ph].
- [24] L.-M. Steinert, P. Osterholz, R. Eberhard, L. Festa, N. Lorenz, Z. Chen, A. Trautmann, and C. Gross, Spatially tunable spin interactions in neutral atom arrays, *Phys. Rev. Lett.* **130**, 243001 (2023).
- [25] C. M. Holland, Y. Lu, and L. W. Cheuk, On-demand entanglement of molecules in a reconfigurable optical tweezer array (2022), arXiv:2210.06309 [cond-mat.quant-gas].
- [26] Y. Bao, S. S. Yu, L. Anderegg, E. Chae, W. Ketterle, K.-K. Ni, and J. M. Doyle, Dipolar spin-exchange and entanglement between molecules in an optical tweezer array (2022), arXiv:2211.09780 [physics.atom-ph].
- [27] J.-R. Li, K. Matsuda, C. Miller, A. N. Carroll, W. G. Tobias, J. S. Higgins, and J. Ye, Tunable itinerant spin dynamics with polar molecules, *Nature* **614**, 70 (2023).
- [28] M. Mizoguchi, Y. Zhang, M. Kunimi, A. Tanaka, S. Takeda, N. Takei, V. Bharti, K. Koyasu, T. Kishimoto, D. Jaksch, A. Glaetzle, M. Kiffner, G. Masella, G. Pupillo, M. Weidemüller, and K. Ohmori, Ultrafast creation of overlapping Rydberg electrons in an atomic BEC and Mott-insulator lattice, *Phys. Rev. Lett.* **124**, 253201 (2020).
- [29] See supplemental material for more details.
- [30] S. Weber, C. Tresp, H. Menke, A. Urvoy, O. Firstenberg, H. P. Büchler, and S. Hofferberth, Calculation of Rydberg interaction potentials, *Journal of Physics B: Atomic, Molecular and Optical Physics* **50**, 133001 (2017).
- [31] N. Šibalić, J. Pritchard, C. Adams, and K. Weatherill, ARC: An open-source library for calculating properties of alkali Rydberg atoms, *Computer Physics Communications* **220**, 319 (2017).
- [32] C. Sommer, G. Pupillo, N. Takei, S. Takeda, A. Tanaka, K. Ohmori, and C. Genes, Time-domain Ramsey interferometry with interacting Rydberg atoms, *Phys. Rev. A* **94**, 053607 (2016).
- [33] H. Hwang, A. Byun, J. Park, S. de Léséleuc, and J. Ahn, Optical tweezers throw and catch single atoms, *Optica* **10**, 401 (2023).
- [34] H. Jo, Y. Song, M. Kim, and J. Ahn, Rydberg atom entanglements in the weak coupling regime, *Phys. Rev. Lett.* **124**, 033603 (2020).
- [35] H. Levine, A. Keesling, A. Omran, H. Bernien, S. Schwartz, A. S. Zibrov, M. Endres, M. Greiner, V. Vuletić, and M. D. Lukin, High-fidelity control and entanglement of Rydberg-atom qubits, *Phys. Rev. Lett.* **121**, 123603 (2018).
- [36] R. Faoro, C. Simonelli, M. Archimi, G. Masella, M. M. Valado, E. Arimondo, R. Mannella, D. Ciampini, and O. Morsch, van der Waals explosion of cold Rydberg clusters, *Phys. Rev. A* **93**, 030701 (2016).
- [37] A. Bergschneider, V. M. Klinkhamer, J. H. Becher, R. Klemt, L. Palm, G. Zürn, S. Jochim, and P. M. Preiss, Experimental characterization of two-particle entanglement through position and momentum correlations, *Nature Physics* **15**, 640 (2019).
- [38] M. O. Brown, S. R. Muleady, W. J. Dworschack, R. J. Lewis-Swan, A. M. Rey, O. Romero-Isart, and C. A. Regal, Time-of-flight quantum tomography of single atom motion (2022), arXiv:2203.03053 [quant-ph].
- [39] U. Haebleren and J. S. Waugh, Coherent averaging effects in magnetic resonance, *Phys. Rev.* **175**, 453 (1968).
- [40] N. Goldman and J. Dalibard, Periodically driven quantum systems: Effective Hamiltonians and engineered gauge fields, *Phys. Rev. X* **4**, 031027 (2014).
- [41] A. Eckardt and E. Anisimovas, High-frequency approximation for periodically driven quantum systems from a Floquet-space perspective, *New Journal of Physics* **17**, 093039 (2015).
- [42] J. Choi, H. Zhou, H. S. Knowles, R. Landig, S. Choi, and M. D. Lukin, Robust dynamic Hamiltonian engineering of many-body spin systems, *Phys. Rev. X* **10**, 031002 (2020).
- [43] Y.-Y. Jau, A. Hankin, T. Keating, I. H. Deutsch, and G. Biedermann, Entangling atomic spins with a Rydberg-dressed spin-flip blockade, *Nature Physics* **12**, 71 (2016).
- [44] E. Guardado-Sanchez, B. M. Spar, P. Schauss, R. Belyansky, J. T. Young, P. Bienias, A. V. Gorshkov, T. Iadecola, and W. S. Bakr, Quench dynamics of a Fermi gas with strong nonlocal interactions, *Phys. Rev. X* **11**, 021036 (2021).
- [45] E. Wigner, On the interaction of electrons in metals, *Phys. Rev.* **46**, 1002 (1934).

## SUPPLEMENTAL MATERIAL

### Rydberg excitation

The unity-filling atomic Mott-insulator is prepared in the  $5S_{1/2}, |F=2, m_F=-2\rangle$  hyperfine ground state of  $^{87}\text{Rb}$  [S1]. We turn off the trapping and optical lattice beams  $\sim 2 \mu\text{s}$  before the Rydberg excitation to avoid multiphoton ionization. We then use two-photon excitation, with picosecond infrared (IR) and blue laser pulses, to excite the ground-state atoms to the  $|29S_{1/2}, m_F=-2\rangle$  Rydberg state. The pulsed laser system for the excitation is as described in ref. [S1].

In detail, we prepare the 29S Rydberg state by using  $\sigma^-$  and  $\sigma^+$  polarized IR and blue pulses as shown in Fig. S5(a). In order to resolve the 29S state from the nearby 27D state, which is only 80 GHz lower in energy, we reduce the excitation bandwidth from previous works by roughly half. At the 29S state resonance (where we perform experiments), the population in the nearby 27D state is found to be only 4 % of the total population which is negligibly small. The laser pulses have an energy of 50 nJ (IR) and 560 nJ (blue), and a  $1/e^2$ -diameter of 230  $\mu\text{m}$  (IR) and 50  $\mu\text{m}$  (blue).

In order to estimate the excitation bandwidth, we excite only the  $|27D_{5/2}, m_F=-4\rangle$  state by using  $\sigma^-$ -polarization for both laser pulses (Fig. S5(a)). A fit to the purple curve in Fig. S5(b) gives a 72(5) GHz (FWHM) bandwidth. In this measurement, the blue pulse energy was reduced to 300 nJ.

### Rydberg state detection

At the end of the experiment, the Rydberg atoms are ionized by a strong electric field, detected by a micro-channel plate (MCP), and counted after going through a pre-amplifier and a time-gated integrator. This detection setup is as described in ref. [S1]. For the field ionization, we applied +2.5 kV pulses to six electrodes (red electrodes in ref. [S2]) and -3 kV pulses to two electrodes (blue electrodes in ref. [S2]).

### Ramsey measurements

The Ramsey measurements are performed by producing a pair of pump and probe pulses with an optical delay-line interferometer [S1]. The pump-probe delay  $\tau$  was tuned by a mechanical stage, whereas the fine delay was controlled with attosecond (as) precision by using a piezoelectric transducer to observe the 1 femtosecond-period Ramsey fringe. We scanned the relative delay in steps of  $\sim 60$  as over a range of  $\sim 3$  femtoseconds, see Fig. S6(a).

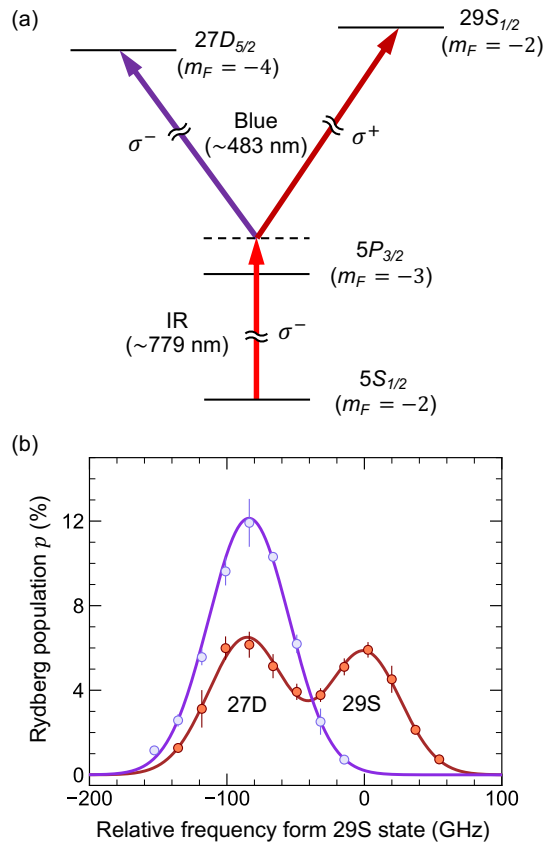


FIG. S5. (a) Scheme for two-photon excitation of 29S and 27D Rydberg states. (b) Example of excitation bandwidth measurement using 27D state (purple data and Gaussian fit). The red data and fit are the same as Fig 1(b).

Experiments are realized on both a Mott-insulator sample, where atoms strongly interact with their neighbours, as well as on a low-density reference sample where interaction can be neglected. This procedure is described in ref. [S1], and allows to extract a phase shift of the Ramsey interferograms between the interacting and reference sample. For the Mott-insulator measurement, the Rydberg population is obtained after sending a single pump-probe pulse for each experimental realization. For the reference measurement, we repeat the pump-probe sequence 150 times, every 1 millisecond, on each low-density sample. This allows to increase statistics and reduce the influence of shot-to-shot uncertainties in pulse energy, pulse pointing and atom number fluctuations. The ion signals are measured after each pair of pump and probe pulses and we record its decrease caused by a depletion of the sample from the finite Rydberg population. This population is extracted by fitting an exponential decay [S2]. By implementing this scheme, there is 30 % reduction in statistical uncertainties for the estimation of contrast and phase of reference sample Ramsey interferograms, as shown in Fig. S6.

The Ramsey signals are measured alternately for the

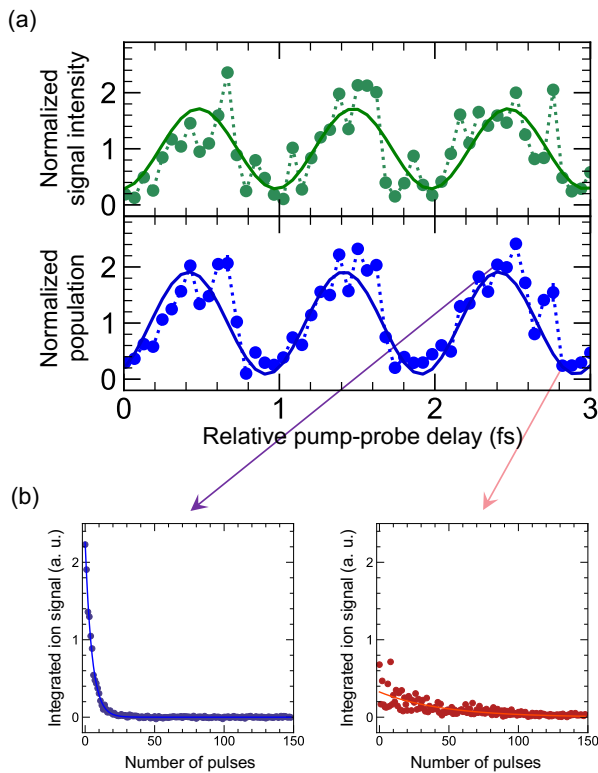


FIG. S6. The Ramsey measurement for reference sample at  $\tau \sim 2.5$  ns. (a) The green points show the measured Rydberg population obtained after one pump-probe pulse, while the blue points are obtained by fitting an exponential decrease, as described in the text. The error bars in blue points show standard deviation. The solid curves show the sinusoidal fit to the data. (b) Examples of Rydberg population estimation at the maximum and minimum of the Ramsey fringe.

reference sample and the Mott-insulator state. Before and after each measurement, we check the number of atoms  $N$  and Rydberg state population  $p$ . We exclude the data with deviations of average values by more than 15 % from the set values:  $N^{\text{set}} \sim 30000$  atoms and  $p^{\text{set}} \sim 4.8\%$ , and 15 % change, as compared to average values, in values recorded after measurement.

### Many-body dynamics for spin-motion coupled system

The Ramsey signal  $P_j$  for an atom  $j$  is given by the following expression [S3]:

$$P_j(\tau) = 2p(1-p)\text{Re}[1 + C_j(\tau)e^{(iE_r\tau/\hbar + \phi_0)}] \quad (\text{S4})$$

Here,  $p$  is the population in the Rydberg state,  $E_r$  is the energy difference between the ground and Rydberg state,  $\tau$  is the pump-probe delay,  $\phi_0$  is a phase arising from the AC-Stark shifts during the pulse excitation, and  $C_j(\tau)$  is interaction-induced modulation of the Ramsey fringe that reflects the coherences established in the

system during the many-body dynamics. The experimentally observed many-particle signal is given by averaging over contributions from all the atoms  $\bar{P}(\tau) = (1/N)\sum_{j=1}^N P_j(\tau)$ .

The term  $C_j(\tau)$  contains the full signature of the interactions, and Ramsey contrast and the phase are related to its absolute value and angle, respectively. For a pure spin-spin model ( $S$ - $S$ ) and just two atoms  $j$  and  $k$ , this term reads:

$$C_{j,k}^{S-S}(\tau) = (1-p) + pe^{iV_{jk}\tau}, \quad (\text{S5})$$

where  $V_{jk}$  is the van der Waals potential between atom  $j$  and  $k$ . This complex-valued term has minimum amplitude for  $V_{jk}\tau = \pi$ , corresponding to maximal spin-spin entanglement. In the special case  $p = 0.5$ , the Ramsey contrast would vanish. For a many-body system, interaction of atom  $j$  with all possible other atoms  $k$  has to be included [S3]:

$$C_j^{S-S}(\tau) = \prod_{k \neq j} [(1-p) + pe^{iV_{jk}\tau}]. \quad (\text{S6})$$

We now include the external degrees of freedom and spin-motion coupling ( $S$ - $M$ ). We first focus on a case of only two atoms  $j$  and  $k$  and obtain:

$$C_{j,k}^{S-M}(\tau) = (1-p) + p\langle \psi_j; \psi_k | e^{iV(\hat{\mathbf{r}})\tau} | \psi_j; \psi_k \rangle, \quad (\text{S7})$$

$$= (1-p) + pO_{jk}(\tau) \quad (\text{S8})$$

where  $|\psi_j\rangle$  describes the spatial wavefunction of atom  $j$ , and  $O_{jk}(\tau)$  is the overlap term introduced in the main text. For atoms localized to an infinitesimal region, the overlap reduces to the previous case  $O_{jk}(\tau) = e^{iV_{jk}\tau}$ .

Extending the calculation to the many-body spin-motion-coupled system is more subtle than for the spin-spin model. Indeed, a strict derivation requires the calculation of terms of higher-order, such as  $O_{jkl} = \langle \psi_j; \psi_k; \psi_l | e^{iV(\hat{\mathbf{r}})\tau} | \psi_j; \psi_k; \psi_l \rangle$ , corresponding to 3 atoms  $j$ ,  $k$  and  $l$  in the Rydberg state. Such higher-order terms do not decompose simply into product of two-body terms, as for the pure spin model. The physical picture being that the momentum kicks on atom  $j$  from two other atoms  $k$  and  $l$  can compensate each other. However, to simplify the calculations, we perform the approximation that higher-order overlaps decomposes into products of two-body overlaps and write:

$$C_j^{S-M}(t) \simeq \prod_{k \neq j} [(1-p) + pO_{jk}(t)]. \quad (\text{S9})$$

We justify this approximation by pointing out that, in our regime of low Rydberg state population ( $p \sim 4.8\%$ ), the dominant error term (3-body overlaps) contributes to a negligibly small fraction  $p$  of the two-body terms. Finally, the calculation over other atoms  $k$  is performed only up to the fourth nearest-neighbor in the 3D lattice (distance  $2a_{\text{lat}}$ ), where the interaction has already dropped by a factor  $2^6 = 64$ .

---

\* vineet@ims.ac.jp

† sylvain@ims.ac.jp

‡ ohmori@ims.ac.jp

[S1] V. Bharti, S. Sugawa, M. Mizoguchi, M. Kunimi, Y. Zhang, S. de Léséleuc, T. Tomita, T. Franz, M. Weidemüller, and K. Ohmori, Picosecond-scale ultrafast many-body dynamics in an ultracold Rydberg-excited atomic Mott insulator, *Phys. Rev. Lett.* **131**, 123201

(2023).

[S2] M. Mizoguchi, Y. Zhang, M. Kunimi, A. Tanaka, S. Takeda, N. Takei, V. Bharti, K. Koyasu, T. Kishimoto, D. Jaksch, A. Glaetzle, M. Kiffner, G. Masella, G. Pupillo, M. Weidemüller, and K. Ohmori, Ultrafast creation of overlapping Rydberg electrons in an atomic BEC and Mott-insulator lattice, *Phys. Rev. Lett.* **124**, 253201 (2020).

[S3] C. Sommer, G. Pupillo, N. Takei, S. Takeda, A. Tanaka, K. Ohmori, and C. Genes, Time-domain Ramsey interferometry with interacting Rydberg atoms, *Phys. Rev. A* **94**, 053607 (2016).